Noname manuscript No.
(will be inserted by the editor)

Dynamical Characteristics of the Piezotronic ZnO Nanowire Device in Ballistic Transport and Its MEMS/NEMS Resonator Hybrid

Leisheng Jin*[1] · Zhi Li[1] · Zongqing Jiang[1] · Lijie Li*[2]

Received: date / Accepted: date

Abstract In this work, the dynamical analysis of carrier transportation in a typical piezoelectric device working in ballistic regime is conducted. Based on the quantum scatting theory, the Poisson and Schrodinger equations are combined for calculating the dynamical transmission coefficient of the a metal-piezoelectric ZnO-metal structure subject to sinusoidal and rectangular external stresses. The roles played by the spanning width of induced piezopotential and incident electron energy in affecting transmission probability are further discussed and clarified, respectively. The cut-off frequency of the piezoelectric device is also studied. Moreover, MEMS/NEMS hybrids specified by double/single-clamped ZnO quantum wire micro/nano-electromechanical resonator hybrids are proposed. Through a comprehensive numerical simulation, it is revealed that the rich nonlinear dynamics of the resonator can be subtly transferred to the piezoelectric device, and the chaotic transmission in the piezoelectric device can arise in two-dimensional parameter space regarding time and incident electron energy. The hybrids, therefore, are endowed with the ability to detect amplitude changes by measuring ultra-sensitive quantum tunneling current. The study sheds light in developing quantum piezotronics and its related MEMS/NEMS integrations.

Keywords piezotronics · ballistic · transmission probabilities · chaos · resonator

L. J et al.
College of Electronic and Optical Engineering & College of Microelectronics, Nanjing University of Posts and Telecommunications, Nanjing 210023, China. E-mail: jinls@njupt.edu.cn

L. L
College of Engineering, Swansea University, Swansea SA1 8EN, UK. E-mail: l.li@swansea.ac.uk

1 Introduction

The piezotronics refers to the field that electronics use inner-crystal piezopotential, which is commonly found in wurtzite structures such as ZnO, GaN, InN and ZnS, as gate voltage to tune/control the charge transport behavior[1][2], and it has found huge applications in self-powered sensors[3], electromechanical memories[4], flexible electronics[5], human-machine interface[6], etc. Currently, the piezotronics is gaining momentum for fabricating ultra-short and ultra-thin devices[7]. This is of necessarily to fulfill the needs for integrating with existing nanotechnologies. More importantly, the pursuit of extreme small piezoelectric device may pave the foundation for developing quantum piezotronics[8], a research branch the piezotronics is rarely but desire to touch. So far, the piezoelectricity in single layer MoS_2 that represents the thinnest piezoelectric device have been reported[9]. The out of plane polarization in graphene-like ZnO nanosheet is revealed by conducting molecular dynamics simulations[10]. The effects brought by piezocharge distribution and Schottky barrier height in a short Ag-ZnO-Ag piezoelectric transistor that spans only dozens of atomic layers are investigated[11]. Flexible phototransistors and gas sensors based on single-layer MoS_2, characterized by fast response and ultrahigh sensitivity, are both experimentally realized[12][13]. ZnO piezotronic transistors with an ultrashort channel length (2 nm) is demonstrated[14], trying to be an alternative to conventional silicon technologies. Heterojunctions made of p-Si/n-CdS (ZnO) ultrashort nanowires are developed successfully as near-infrared photodetectors[15], which performs orders higher of photoresponsivity and detectivity than traditional ones. These works have witnessed the filed of piezotronics for continuous miniaturization and developing novel applications in a wide range of areas. Nevertheless, Challenges arise along the road to realize the quantum piezotronics and make the peizoelectric devices more compatible with state-of-the-art technologies.[7][8]. First, most of the existing works are restricted for studying low-frequency and static cases that the piezopotential induced is seen monotonously as a constant change of Schottky barrier at the interface between electrodes and wurtzite materials, and the classical Schottky theory is heavily dependent for analyzing the carrier transportation[16][17]. This is though reasonable as the external applied stress with low-frequency hardly bring effect to the ultra-fast electron transporting process. However, when the strains induced are with a high frequency the dynamical analysis are still missing and highly demanded. Second, piezoelectric devices are prone to be studied in circumstances that external strains come deliberately[9][14]. This somehow hampers for the development of integrable piezoelectric devices. Given that the piezotronics is of desire to merge into the current advanced technologies such as MEMS/NEMS, CMOS[7], etc, the induced strains in charge of generating piezopotential to "gate" the carries transportation should ideally find its sources from the platforms they are integrated with, and therefore issues on how to couple the piezoelectric devices with the existing electronic platforms should be addressed.

Here, we focus on the ballistic transport regime of the piezotronics, which represents one of the ultimate targets in developing ultra-small piezoelectric device. Particularly, we study the dynamical characteristics of a typical two-terminal piezoelectric device. The traditional Schottky barrier models widely taken for calculating the current-voltage relations in piezotronics are left aside. Alternatively, a Poisson equation and Schrodinger equation coupled model is employed, by which the piezopotential varies according to the dynamical external stresses rather than taking as a constant value, and the Schottky barrier gates the wave-like carriers' transportation in dynamical form. The roles of the spanning width of induced piezopotential and cutoff frequency of the two-terminal piezoelectric device are discussed and clarified in depth. Moreover, we conceive the scenarios of which the piezoelectric device working in ballistic regime integrates with two general types of MEMS/NEMS resonators. The resonators can work with high frequency, and that the piezoelectric device receives dynamical stress from the resonator instantly, which can exhibit a rich nonlinear dynamics such as chaos. By conducting comprehensive numerical analysis, the nonlinear dynamics of the electron transportation in quantum piezoelectric device is for the first time characterized. The proposed hybrids can shed light in developing MEMS/NEMS-piezotronics integration technology, and has potential applications in sensing areas.

2 Theoretical Model

The studied Metal-ZnO-Metal structure is shown in Fig. 1 (a). Here, the metals, working as electrodes, can be taken as different materials (e.g., Ag, Cu) so that the two contacts between metals and semiconductor may form ohmic or Schottky type[18], and in this work we focus on the general case that the left contact is Schottky type and the right contact is ohmic. The energy band diagram of the Schottky contact is given in Fig.1 (b), in which the Schottky barrier, closely related to the induced piezopotential, changes up and down (indicated by the red arrow) according to external strains that might be applied in any forms of varying functions with low or high frequency. The ZnO nanowire is assumed to be ultra-short for satisfying the ballistic transport regime, and that the current flowing in the ballistic ZnO nanowire is given by Landauer theory[19]:

$$I = \frac{2q}{h} \int T(E)M(E)(f_1(E) - f_2(E))dE \tag{1}$$

where the h is Plank constant, q is the elementary charge, T represents the transmission probability of an electron incident from the left electrode to the right electrode, $M(E)$ is the number of transport channels, and in our one-dimensional ZnO model the $M(E)$ is always 1. f_1 and f_2 are Fermi functions in the left and right terminal. When there is an external voltage applied to the left and right electrodes, the "fermi window" ($f_1(E)$-$f_2(E)$) opens, and electrons with energy states belonging to this window are likely to tunnel

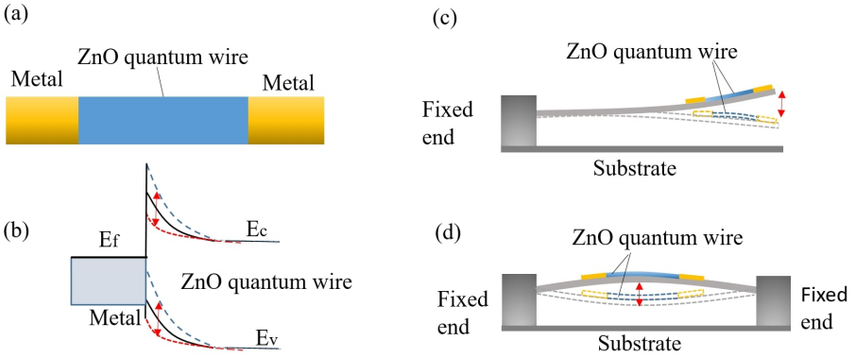

Fig. 1 (a) Schematic diagram of the studied metal-ZnO-metal structure. (b) Band diagram of metal-Zno interface with dynamically changing Schottky barrier shown. (c) and (d) are schematic diagrams of single/double clamped nano-electromechanical resonator and Zno nanowire hybrid, respectively.

through the short ZnO nanowire. It is obvious that, based on the Eq. (1), the transmission T is the core parameter if one wants to calculate the current. In this work, we adopt a method that can be used to calculate the transmission coefficient with arbitrary potential barrier[20]. Specifically, the ZnO nanowire is treated as potential barrier for the electrons ready to tunnel through, where the potential energy distribution depends on the voltage applied between the left and right electrode and the piezopotential generated by external strains. The transmission T can be calculated by dividing the potential barrier into N small rectangles, as shown in Fig. 2. The potential energy of j^{th} segment is given by $U(z_j) = V[(z_{j-1} + z_j)/2]$, where $j = (1, 2, 3, ..., N, N+1)$ is the number of the segment. One can see that if N is large enough, the potential function in the nanowire can be recovered. In a single rectangular potential barrier j, the time independent wave function of an electron can be described by the Schrödinger equation:

$$E\Psi z_j + \frac{\hbar^2}{2m}\frac{d^2\Psi(z_j)}{dx^2} - U(z_j)\Psi(z_j) = 0 \tag{2}$$

where E is the overall energy of an indecent electron. m is the rest mass of an electron. The wave function Ψ_j of the j_{th} segment is derived straightforwardly, as:

$$\Psi(j) = A_j e^{ik_j z} + B_j e^{-ik_j z} \tag{3}$$

where $k_j = \sqrt{[2m(E - U(z_j))]}/\hbar$. According to the theory of quantum mechanics, the Ψ and $d\Psi_j/dz$ should be continuous at boundaries between divided segments, from which the amplitudes A_j and B_j can be determined by:

$$\begin{pmatrix} A_j \\ B_j \end{pmatrix} = \prod_{l=0}^{j=1} M_l \begin{pmatrix} A_0 \\ B_0 \end{pmatrix} \tag{4}$$

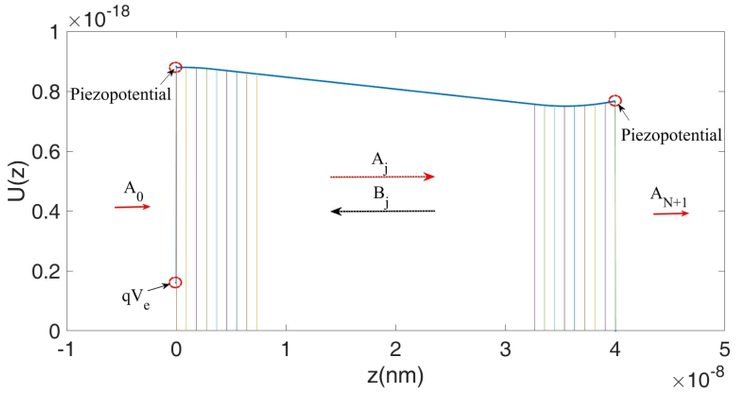

Fig. 2 Potential energy distribution over the metal-ZnO-metal structure when external voltage applied. The potential energy function can be seen as N rectangular barriers which are partially drawn. A_0, A_j and A_{N+1} represent amplitudes of incident wave that is before injecting the interface of M-ZnO, inside of ZnO and at the right ZnO-M interface.

where M_l is given by:

$$M_l = \begin{bmatrix} (1+s_l)e^{[-i(k_{l+1}-k_l)z_l]} & (1-s_l)e^{[-i(k_{l+1}+k_l)z_l]} \\ (1-s_l)e^{[i(k_{l+1}+k_l)z_l]} & (1+s_l)e^{[i(k_{l+1}-k_l)z_l]} \end{bmatrix} \tag{5}$$

In Eq. (5), $S_l = k_l/k_{l+1}$. The scatting matrix M can then be obtained as:

$$M = \begin{bmatrix} M_{11} & M_{12} \\ M_{21} & M_{22} \end{bmatrix} = \prod_{l=0}^{N} M_l \tag{6}$$

Finally, the transmission T can be calculated as follows: $T = k_{N+1}/k_0|k_0/(k_{N+1})M_{22}|$, provided by setting $A_0 = 1$ and $B_{N+1} = 0$. Next, the potential energy function in the ZnO nanowire needs to be further clarified. We take the parallel plate capacitor model for calculating the potential energy inside the ZnO when there is external voltage applied to the source and drain electrodes, i.e., the potential energy in the nanowire is given by $V_w(z) - qV_eC_D(z)/C_{ES}(z)$, where V_e is the voltage applied to the ZnO nanowire, $C_{ES} = C_D + C_S$ is the total electrostatic capacitance at point z, and C_D (C_S) is the capacitances linking the point at z to drain (source). V_{w0} is the initial potential energy in the quantum wire calculated from reference point of zero potential energy. Ignoring the charging effect in nanowire, the $V_w(z)$ can be explicitly expressed as:

$$V_w(z) = V_{w0} - qV_e\frac{1/C_s(z)}{1/C_D(z) + 1/C_s(z)} = V_{w0} - qV_e\frac{z}{L_z} \tag{7}$$

During the derivation of Eq. (7), the relations $C_s(z) = \varepsilon A/z$ and $C_D(z) = \varepsilon A/(L_z - z)$ have been used, where ε and A represents the permittivity and cross-section area of the nanowire, respectively.

3 Numerical Simulation

In the following numerical simulations, the source and right drain electrodes of the device are assumed to be reservoirs of electrons, i.e., the electrons are keeping presumably in equilibrium state, even under a given applied voltage. The potential inside of the electrodes is approximately constant all the time while the potential at the boundaries is higher which confines the electrons. The electrons in the electrode tunneling through the ZnO nanowire are always supposed to have the fermi energy E_F unless specific incident electron energy assumed.

3.1 Sinusoidal and Rectangular Changing Stress Applied

Here, we consider the cases in which the ZnO nanowire is dynamically compressed and stretched, and there are strains generated accordingly. Due to the piezoelectric property of the ZnO nanowire, equivalent positive and negative piezoelectric charges are induced at each interface of the metal-nanowire. Assuming that the induced piezoelectric charge has density ρ_p and spans over width z_{pl} and z_{pr} at left and right interface, the piezopotential can be obtained by using the Poisson equation:

$$-\frac{d^2V_p(z)}{dz^2} = q\frac{\rho_p(z)}{\varepsilon_s}, z_l \leq z \leq z_{pl}; z_{pr} \leq z \leq z_r \tag{8}$$

Generally, the z_{pl} and z_{pr} is in reality very narrow, i.e., $z_{pl} \ll L_z$ and $z_{pr} \ll L_z$, which makes the piezopotential variation over the width z_{pl} and z_{pr} negligible. In specific calculations, we take the parameters as follows[16]. The piezoelectric constant $e_{31} = -0.51$ C/m^2, $e_{33} = 1.22$ C/m^2 and $e_{15} = -0.45$ C/m^2. The relative dielectric constant $\varepsilon_s = 8.91$. the material of the left and right electrode are taken as Ag and Cu, respectively. The donor density of N_d in the ZnO is 1×10^{16}/cm^3. The built-in potential of the Schottky barrier $\phi_b = 0.3$ eV.

First, we suppose that the strain induced on the nanowire has the sinusoidal changing: $S_{33} = S_{330}sin(\omega t)$, with the amplitude $S_{330} = 0.4/100$ and $\omega = 100$ Hz. The transmission probability of an electron incident from the left electrode, when the applied voltage to source and drain varies in the range of [0 1] V, is calculated by combining Eqs. 2-8. We can see from the Fig. 3 (a) that the generated piezopotential varies according to the sinusoidal changing strains, with amplitude about 0.1 V. In Fig. 3 (b), a typical result of transmission probability vs applied voltage V_e at $t = 0.249$ s is presented, in which it is seen that as the V_e goes up the transmission probability becomes nonzero at approximately $V = 0.2$ V, and gradually increases to nearly 1 after going through a short fluctuating interval in [0.2 0.21] V. In addition, one can see that there are a few quantum resonances appearing after the V_e get larger than about 0.518 V, in which the lower part of quantum resonances has a larger Q factor. This is consistent with the theory of the quantum resonance. To further

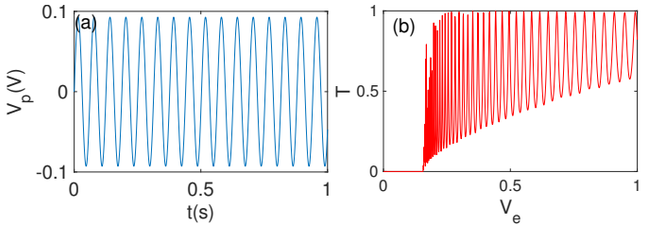

Fig. 3 (a) The generated piezopotential vs time when sinusoidal changing external strain applied. (b) Typical result of transmission probability vs applied voltage V_e at $t = 0.249$.

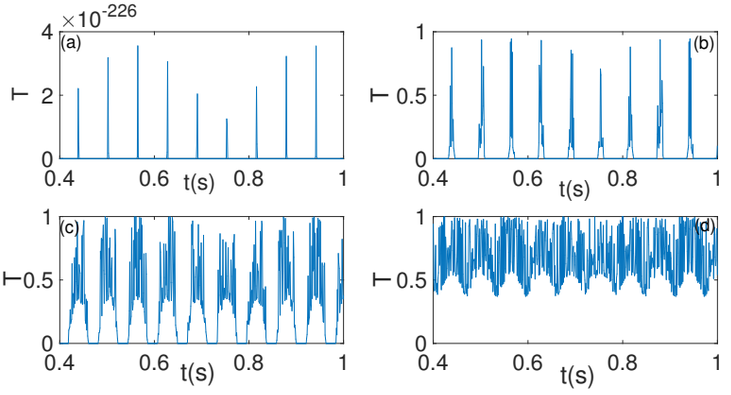

Fig. 4 Dynamical transmissions vs time at certain applied voltages. (a) $V_e = 0.1$ V; $V_e = 0.2$ V in (b); $V_e = 0.5$ V in (c) and $V_e = 0.9$ V in (d).

illustrate the dynamical processes of how the transmission probability changes with the time-varied external strains, we calculate the dynamical transmission when V_e = 0.1 V, 0.2 V, 0.5 V and 0.9 V, as shown in Fig. 4 (a), (b), (c) and (d). In Fig. 4 (a), some transmission peaks with extreme low probabilities around 2×10^{-226} appear at points where the largest piezopotential is induced. When V_e is increased to 0.2 V and 0.5 V, respectively, there are more points around the peak of the induced piezopotential appear but with a much more high probabilities. In Fig. 4 (d), when the V_e = 0.9 V, corresponding to the range where quantum resonances occurring, it is shown that nearly all the points during the dynamical time interval are with comparable transmission probabilities, and the transmission curve shows ups and downs surrounding to the peaks of the induced piezopotential, which is because of the double periodic effect originating from quantum resonances and external induced strains (or piezopotentials).

Likewise, the case of induced external strains changing dynamically in rectangular shape is also investigated, and the results of generated piezopotential and a typical transmission calculation vs applied voltage V_e at t = 0.27 s are presented in Fig. 5 (a) and (b), respectively. In Fig. 5 (a), the generated piezopotential are in accordance with induced external strains on ZnO

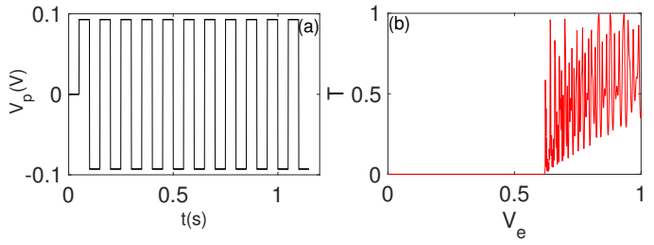

Fig. 5 (a) The generated piezopotential vs time when rectangular changing external strain applied. (b) Typical transmission calculation vs applied voltage V_e at $t = 0.27$.

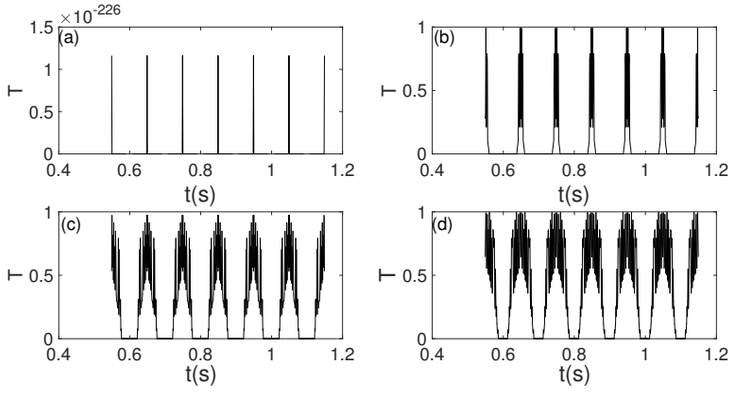

Fig. 6 Dynamical transmission calculations of Zno nanowire subjected by rectangular changing external strains. (a) $V_e = 0.1$ V; (b) $V_e = 0.4$ V; (c) $V_e = 0.8$ V; (d) $V_e = 1$ V.

nanowire characterized by duty ratio: 50/100 and amplitude: $S_{330} = 0.4/100$, and the transition probability versus V_e shows a more fluctuating quantum resonances, compared with the above sinusoidal case (see the result shown in Fig. 3 (b)), after the threshold of nonzero transmission probability at about $V_e = 0.62$ V. We further conduct the investigation of dynamical transmission subjected by the rectangular changing strains. The results of dynamical transmission calculations at $V_e = 0.1$ V, 0.4 V, 0.8 V and 1 V are given in Fig. 6 (a), (b), (c) and (d). We can see apart from the phenomenon that more and more points around the top of the square wave get with large transmission probabilities, the nonzero probabilities are in axis symmetry that the fluctuating probabilities on two sides of the symmetry axis are exactly the same.

3.2 Piezopotential Width Dependant Transmission

In the last section, the dynamical transmission probability of an incident electron with fermi energy under the sinusoidal and rectangular changing strains

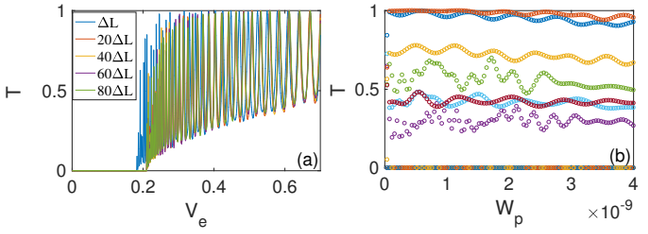

Fig. 7 (a) Transmission probabilities vs applied voltage under different piezopotential width spanning. (b) Piezopotential width W_p dependant transmissions with V_e setting at certain values in range of [0 1]V.

are investigated. It is worthy to mention that a constant spanninig width W_p ($W_p = \Delta L = Lz/N, N = 1000$) of the induced piezopotential is assumed. Here, we study of how the width of piezopotential spanning affect the transmission coefficients. Specifically, a static external strain ($S_{330} = 0.5/100$) is applied, then the transmission probability is calculated by setting the piezopotential width spanning over $\Delta L, 2\Delta L, 3\Delta L, ..., 100\Delta L$, all with V_e varying in [0 1] V. The results of $W_p = \Delta L, 20\Delta L, 60\Delta L, 80\Delta L$ are given in Fig. 7 (a). It can be seen that the thresholds for having nonzero transmission probability is delayed for $W_p = 20\Delta L \sim 80\Delta L$ compared with $W_p = \Delta L$, and there is an oblivious quantum resonance shift in the latter part of $V_e \in [0.72\ 1]$ V between $W_p = \Delta L$ and the rest curves. To further understand this point, we calculate the W_p dependant transmission by fixing the V_e at a few certain values in [0 1] V, and the results are shown in Fig. 7 (b). We can see that the transmission probabilities are with fluctuations at smaller W_p, and as the W_p gets wider, e.g., $W_p \in$ [3 4] nm, the transmission probabilities get flatter. However, this may not work for higher values of V_e which always has neat ups and downs as shown in the upper part of the Fig. 7 (b). Combining both Fig.7 (a) and Fig. 7 (b), it is concluded that the spanning width of piezopotential plays a more important role when itself is small as well as the peizoelectric device is applied with a low bias. In addition, the consequence brought by the width changing is not linear.

3.3 Transmission Probability vs Incident Electron Energy

The dynamical transmission calculation of the incident electron with different energy is conducted in this section. In the simulation, we set the $V_e = 0.5$ V, the electron energy E_x varying in [4 6] eV, and the external inducted strains varying in sinusoidal function: $S_{33} = S_{330}sin(\omega t)$ with $S_{330} = 0.7/100$ and $\omega = 1$ KHz. The result is shown in Fig. 8 and Fig. 9, respectively. In Fig. 8 (a), (b) and (c), we plot the transmission coefficients versus time when $E_x = 4.7$ eV, $E_x = 4.9$ eV and $E_x = 5.2$ eV, where it can be seen that the transmission starts with a few spikes with very low probabilities at $E_x = 4.7$ eV, followed by more spikes with larger probabilities occurring as E_x increased

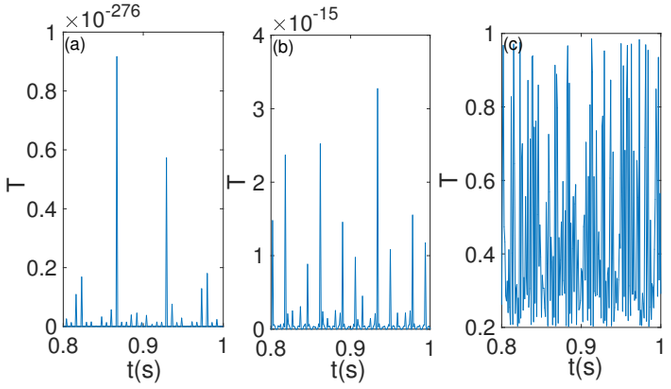

Fig. 8 Dynamical transmission calculations of incident electron with different energy when inducted strains varying sinusoidally. (a) $E_x = 4.7$ eV; (b) $E_x = 4.9$ eV; (c) $E_x = 5.2$ eV.

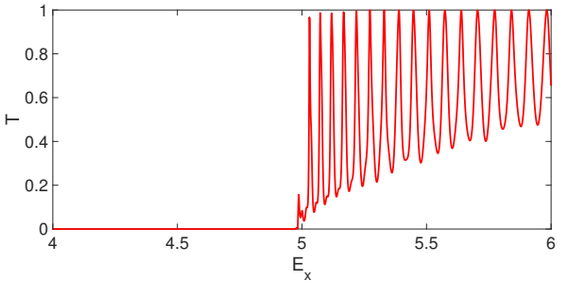

Fig. 9 Transmission probabilities versus incident electron energy E_x at $t = 0.25$.

to 4.9 eV, and finally when $E_x = 5.2$ eV the transmission of the incoming electron fluctuate like in chaotic state, even though the induced strains at the moment on ZnO nanowire in periodic. This can be explained by that: when the energy of the incident electron is relatively large, the transmission might be fluctuating. In the numerical simulation, the induced strains of sinusoidal changing are taken discretely in each period, and the tiny differences between adjacent taken points are amplified in calculating transmission probabilities. In Fig. 9, the transmission at $t = 0.25$ s versus incident electron energy E_x is plotted, in which quantum resonances are shown but with no oblivious differences from the result in Fig. 3 (b).

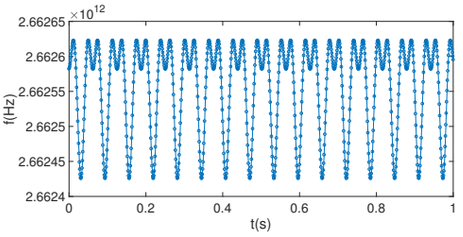

Fig. 10 The changing cut-off frequency when induced strains varying sinusoidally at V_e = 0.9 V.

3.4 Analysis of Frequency Limitation on External stress

The cutoff frequency of the ballistic ZnO nanowire indicates the largest frequency an dynamical external strain can be applied. It is defined by:

$$f_{cutoff} = \frac{1}{2\pi T_{avg}} \tag{9}$$

where $T_{avg} = Lz/\sum_{i=1}^{N}(k_i\hbar/m_0)/N$ represents the average time of tunneling events, and the k_i represents the wave number of the i^{th} segment divided while calculating the transmission. m_0 is the rest mass of an electron. We calculate the cutoff frequency when there is dynamical induced strains ($S_{33} = S_{330}sin(\omega t)$, $S_{330} = 0.4/100$ and $\omega = 100$ Hz.). The result of the $V_e = 0.9$ V is shown in Fig. 10. It is seen that under sinusoidal changing strains the cutoff frequency shows two valleys in each period valued around 2.6625 THz.

3.5 ZnO-Micro/Nano Electromechanical Resonator Hybrid

Various kinds of nano-electromechanical resonators have been experimentally realized in previous works[21][22][23]. Here, we take the one constructed by a suspended doubly clamped beam as the first example of piezo-resonator hybrid. The schematic diagram is shown in Fig. 1 (d). The resonator is driven by electrostatic force and can work with frequency as high as GHz. Its in-plane displacement $y(t)$ can be described by a well-established model, which gives:

$$\ddot{y}(t) + \omega_0^2 y(t) + \delta\dot{y}(t) + \alpha y^3(t) = 2F_0 cos(\omega_d t) \tag{10}$$

where $\delta = \frac{-f_1}{\rho S}$ denotes the damping ratio, $f_1 = \pi pT/(4v_t)$ and $v_t = \sqrt{k_b Tm}$. $\alpha = 8E\pi^4/(9\rho L^4)$ is Duffing coefficient and $F_0 = \sqrt{2/3}f_0/(\rho S)$ is external driving amplitude with $f_0 = \pi\varepsilon V_{dc}V_{ac}/(h(ln(4h/d)^2))$. The ω_0 and ω_d are natural frequency and driving frequency, respectively. The length, thickness and width of the resonator are taken to be 3 μm, 50 nm and 150 nm. The material is taken to be silicon. Detailed description of the model can be found in[24]. The resonator exhibits dynamics with certain periodicity under different driving strengths achieved by applying appropriate V_{dc} and V_{ac}. In this case,

Table 1 Parameters for the nano-electromechanical resonator

Symbols	Values	Units
T, W, L	50, 150, 3000	nm
ρ	2322	kg/m^3
E	169	Gpa
V_{dc}, V_{ac}	5,5	V
h, d	1000, 50	nm
ε	8.85×10^{-12}	F/m
T	300	K
p	1.01325×10^5	Pa
m	5.6×10^{-26}	kg
k_b	1.38×10^{-23}	J/K

we only focus on period-1 variation by setting $V_{dc} = 5$ V and $V_{ac} = 5$ V. During the vibration, the ballistic ZnO nanowire attached closely on the top surface of the resonator beam is stretched and compressed accordingly, and there are dynamical strains together with peizopotential being induced. The inducing z-axis strains ε_z are given by:

$$\varepsilon_z = -\frac{M}{(E_p I_p + E_b I_b)}\left(y_n - \frac{T_p}{2}\right) \tag{11}$$

where $E_{p,(b)}$ and $I_{p,(b)}$ are Young's modulus and inertia moment of the nanowire (resonator beam), respectively. M is the moment generated during the vibration of resonator and y_n is distance to the neutral axis, and they can be calculated by:

$$M = E_b I_b \kappa \tag{12}$$

$$y_n = \frac{\frac{T_p}{2} T_p \frac{E_p}{E_b} + \left(T_p + \frac{T_b}{2}\right) T_b}{T_p \frac{E_p}{E_b} + T_b} \tag{13}$$

where $T_{p,(b)}$ is the thickness of the nanowire and resonator beam, respectively. κ is the curvature, which is dynamically related to the displacement of the resonator. By taking the boundary conditions that $y(t)_{z=0} = y(t)_{z=L_b} = 0$, the curvature is given by:

$$\kappa = sign(y(t)) \frac{8}{((L_b^2 + 4y(t)^2)^2 / y(t)^2)^{1/2}} \tag{14}$$

Combining Eqs. (2-8) and Eqs. (9-13), the dynamical $y(t)$ and transmissions are calculated when the energy E_x of the incident electron varying in the range of [4 6] eV and $V_e = 0.5$ V, as shown in Fig. 11. In Fig. 11 (a), the displacement $y(t)$ is oscillating in period-1 state as we expect. The dynamical transmission probabilities at $E_x = 4.75$ eV, $E_x = 5$ eV, $E_x = 5.5$ eV and $E_x = 6.25$ eV are presented in Fig. 11 (b), (c), (d) and (e). Interestingly, it is seen that at different energy E_x the transmission probabilities in one period exhibit different periodicity. This is attributed to that there are different

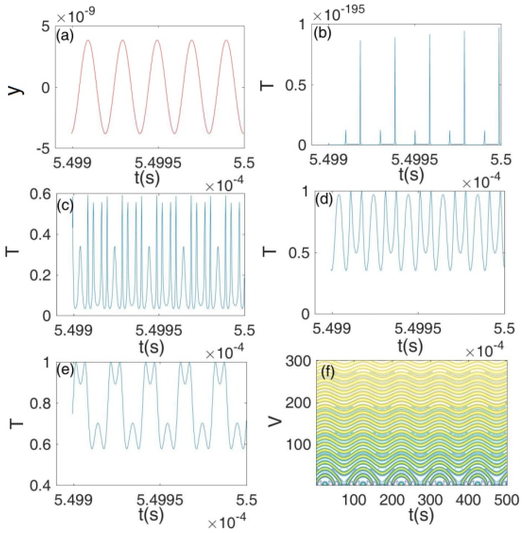

Fig. 11 Transmission studies of double-clamped piezo-resonator hybrid. (a) Time series of displacement $y(t)$ in period-1. (b) Transmission probabilities vs time at $E_x = 4.75$ eV; (c) Transmission probabilities vs time at $E_x = 5$ eV; (d) Transmission probabilities vs time at $E_x = 5.5$ eV; (e) Transmission probabilities vs time at $E_x = 6.25$ eV; (f) Dynamical Transmission over a certain time interval with $E_x \in$ [5 6.5] eV.

quantum resonances existing at different E_x , and the quantum resonances can modulate the transmission periodically, during which the larger strains induced in one time-period could possibly lead smaller transmission probabilities. To have a whole picture of the transmission in a continuous range of $E_x \in [5 \quad 6.5]$ eV, we present the contour of the transmission over a certain time interval in Fig. 11 (f). It can be seen that as the periodicity evolves into period-1 as E_x goes up, the transmission probabilities reach about 1 (light yellow color at the top).

The hybrid of ballistic ZnO nanowire with a single-clamped electromechanical resonator is also conceived and investigated. As shown in Fig. 1 (c), the nanowire is fabricated on the free end of the resonator. When the resonator vibrates, the nanowire is subjected to stretched and compressed stresses which bring z-axis dynamical strains and piezopotentials. To be general, we, here, put a well-known model for describing the dynamics of the resonator[25]. The model is given by:

$$\ddot{y} + \delta\dot{y} + \beta y + \alpha y^3 = \gamma cos\omega t \tag{15}$$

where δ is damping ratio, β and α are linear and cubic spring constant, respectively. γ is the amplitude of external driving with frequency ω. It should be noted that all these parameters are dimensionless. Detailed arguments on the parameter can be found in quite a few references[25]. In the following simulation, the parameters are taken as: $\delta = 0.2$, $\alpha = 1$, $\gamma = 0.3$ and $\omega = 1$. Particularly, the β is taken as negative, i.e., $\beta = -1$. It is known that when

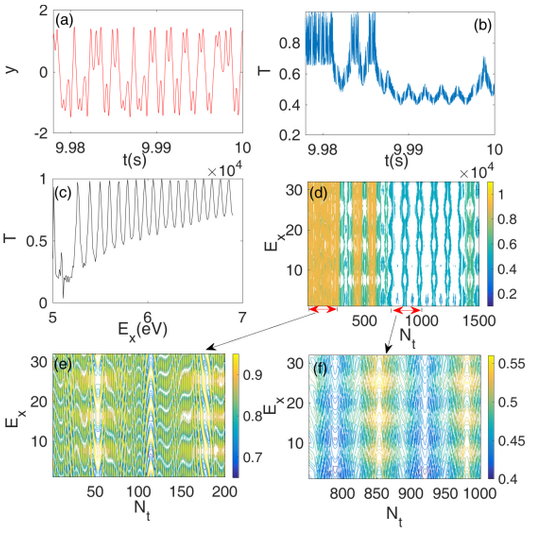

Fig. 12 Dynamical transmission in hybrid of ballistic ZnO nanowire with single-clamped electromechanical resonator. (a) The chaotic time series of the hybrid in time interval [9.978 10]s; (b) The transmission calculation of ZnO nanowire in the hybrid with incident energy $E_x = 6.7$; (c) Typical transmission with quantum resonances versus E_x. (d) Contour diagrams of transmissions with E_x varying in [6.6 6.9] eV in time range of [9.978 10]s; (e) Partial plotting of (d) with N_t in [1 200]; (f) Partial plotting of (c) with N_t in [750 1000].

the spring constant is negative the resonator can exhibit rich nonlinear dynamics such as chaos, which also happens to be our focus in this part. For single-clamped resonators, the induced strains on the ZnO nanowire is with linear relation with the displacement of the resonator, i.e., $\varepsilon_z = Cy(t)$. When the energy of the incident electron E_x varying in the range [5 6.9] eV, the transmission probabilities under the chaotic state of the resonator are calculated based on the Eqs. 2-8 and Eq. 15, and the results are presented in Fig. 12. The chaotic time series in time interval [9.978 10]s is plotted in Fig. 12 (a) and the transmission calculation of $E_x = 6.7$ eV in the same time interval is given in Fig. 12 (b). Seeing from these two plots, one can find some correlations in between by comparing the trajectories. For example, in time interval [9.99 9.995]s the displacement trajectories can be divided in to four similar shapes, and that in the same time interval there are four corresponding transmission appeared in Fig. 12 (b). In Fig. 12 (c), a typical transmission with quantum resonances versus E_x is presented, which illustrates that the dynamical transmission is also modulated by quantum resonances. Furthermore, we calculate the two-dimensional contour diagrams of transmissions in the same time range of [9.978 10]s, which is divided into 1500 small time intervals, with E_x varying in [6.6 6.9] eV. The overall result is shown in Fig. 12 (d), with partial plotting of N_t in [1 200] and N_t in [750 1000] given in Fig. 12 (e) and (f) as indicated by the arrows, respectively, where N_t is the

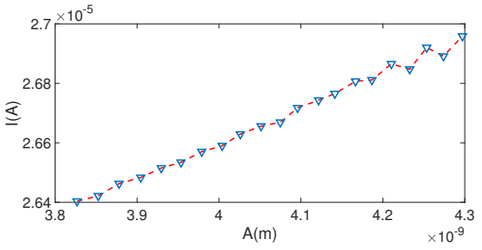

Fig. 13 The tunneling current I vs amplitude of double-clamped piezo-resonator hybrid.

number location in the 1500 small time intervals. It can be seen in the Fig. 12 (d) that both spatiotemporal chaotic and periodical states appear. This is essentially consist with the result shown in Fig. 12 (b) that in the fist part of time range of [9.978 10]s (i.e., N_t in [1 200]) the chaotic displacements corresponds to chaotic transmissions, and wherever the rest part of the same time range the chaotic displacements lead to periodical-like transmissions, which is distinguished with the double-clamped piezo-resonator hybrid studied above that periodical displacement can only lead to periodical transmissions. The reason for this is that the chaotic state, essentially, is with many unstable periodical states embedded, and the displacements of unstable periodical states have different frequencies, which together with the existing quantum resonances co-modulate the strains and piezopotentials in the ZnO nanowire that can directly shift the transmissions in and out the chaotic state.

Last but not the least, we investigate how the changing amplitudes affect the tunneled current in ballistic ZnO nanowire. In practical view, this is actually related to the sensing applications, e.g., mass sensors, based on nanoelectromechanical resonators. Supposing that there is a tiny mass adhered to the resonator beam, the amplitude of the resonator changes, so is the tunneled current. Here, we calculate the tunneling current versus varying amplitudes of the doubly clamped resonator studied above. The tunneling current is given by: $I = -q^2 V_e/(\pi\hbar)T$. By combining Eqs. (1-8, 10-14), the tunneling current I when amplitude varying in [3.8 4.3]nm is calculated, and the result is presented in Fig. 13. It can be seen that the there is linear relation between the amplitude and tunneling current, further proving that the piezo-resonator hybrid has the potential in developing high sensitivity sensors.

4 Conclusion and Discussion

The dynamical electron transmission in an ultra-short two-terminal piezoelectronic device working in ballistic regime is analyzed. An universal model that can be used for calculating the transmission coefficient of the piezoelectronic device subject to arbitrary eternal dynamical stresses is developed. Both the spanning width of induced piezopotential and incident electron energy are confirmed for playing an important role in affecting the quantum transmis-

sion of the device. The cut-off frequency of the piezoelectronic device is also discussed. Hybrids which integrate MEMS/NEMS resonators with the piezoelectronic device in ballistic regime are proposed and studied. Numerical simulations show that the coupled device is of capability for transferring the rich nonlinear dynamics, particularly the chaos, of the resonator to the piezoelectronic device. There are a few merits of the work worthy to mention. First, the study paves the way for developing quantum piezotronics working in ballistic regime, a research branch the piezotronics is not yet well developed in the sense of dynamical models and theories. This work provides insight on how the extreme small piezoelectronic device perform in arbitrary dynamical environment, which could further inspire the novel applications exploration based on quantum piezoelectric devices. Second, the proposed hybrids can shed light in realizing MEMS/NEMS integrated piezotronics. In practical, the MEMS/NEMS resonators are widely used for sensing. Integrating the peizoelectric device in ballistic regime with the resonator can facilitate the resonator to receive electrical signal more directly and sensitively. Third, the work establishes an approach for exploring/utilizing complex dynamics in piezotronics[26]. Traditionally, the piezoelectronic devices are often studied when only static external stresses applied, and it seems there are no nonlinear dynamics in piezotronics reported so far. The hybrids proposed here can be served as a controllable and effective mean for providing diversified external strain/stress to fabricated piezoelectronic devices, which will stimulate the cross-research of piezotronics and nonlinear dynamics, such as chaos, both in theories and applications.

Acknowledgment

This authors acknowledge the funding supported by China Postdoctoral Science Foundation (2019T120447)

DATA AVAILABLITY

The data that support the findings of this study are available from the corresponding author upon reasonable request.

References

1. Zhong Lin Wang, "Nanopiezotronics", Advanced Materials, vol. 19, pp. 889-992, 2007
2. Rodolfo Araneo, Senior Member, Fabiano Bini, Marialilia Pea, Andrea Notargiacomo, Antonio Rinaldi, and Salvatore Celozzi, "Impact of Non-Linear Piezoelectricity on the Piezotronic Effect of ZnO Nanowires", IEEE transactions on nanotechnology, vol. 15(3), pp. 512-520, 2016
3. Sheng Xu, Yong Qin, Chen Xu, Yaguang Wei, Rusen Yang, Zhong Lin Wang, "Self-powered nanowire devices", Nature Nanotechnology, vol. 5, pp. 366-373, 2010
4. Wenzhuo Wu, Zhong Lin Wang, "Piezotronic nanowire based resistive switches as programmable electromechanical memories", Nano Lett., vol. 11, pp. 2779-2885, 2011

5. Wei Li, David Torres, Ramon Diaz, Zhengjun Wang, Changsheng Wu, Chuan Wang, Zhong Lin Wang, Nelson Sepulveda, "Nanogenerator-based dual-functional and self-powered thin patch loudspeaker or microphone for flexible electronics", Nature Communications, vol. 8:15310, 2017
6. Qilin Hua, Junlu Sun, Haitao Liu, Rongrong Bao, Ruomeng Yu, Junyi Zhai, Caofeng Pan, Zhong Lin Wang, "Skin-inspired highly stretchable and conformable matrix networks for multifunctional sensing", Nature Communications, vol. 9:244, 2018
7. Caofeng Pan, Junyi Zhai, Zhong Lin Wang, "Piezotronics and Piezo-phototronics of Third Generation Semiconductor Nanowires", Chemical Reviews vol. 119(15),2019
8. Laipan Zhu, ZhongLin Wang, "Progress in piezotronics and piezo-phototronics of quantum materials", Journal of Physics D: Applied Physics, vol. 52:343001, 2019
9. Wenzhuo Wu, Lei Wang, Yilei Li, Fan Zhang, Long Lin, Simiao Niu, Daniel Chenet, Xian Zhang, Yufeng Hao, Tony F. Heinz, James Hone, Zhong Lin Wang, "Piezoelectricity of single-atomic-layer MoS_2 for energy conversion and piezotronics", Nature, vol. 514, pp. 470-477, 2014
10. Dan Tan, Morten Willatzen, and Zhong Lin Wang, "Out-of-Plane Polarization in Bent Graphene-Like Zinc Oxide and Nanogenerator Applications", Adv. Funct. Mater. vol. 30(1907885), 2020
11. Wei Liu, Aihua Zhang, Yan Zhang, Zhong Lin Wang, "Density functional studies on wurtzite piezotronic transistors: influence of different semiconductors and metals on piezoelectric charge distribution and Schottky barrier", Nanotechnology, vol. 27:205204, 2016
12. Pei Lin, Laipan Zhu, Ding Li, Zhong Lin Wang, "Defect repair for enhanced piezo-phototronic MoS_2 flexible phototransistors", Journal of Materials Chemistry C, vol. 7:14731, 2019
13. Junmeng Guo, Rongmei Wen, Junyi Zhai and Zhong Lin Wang, "Enhanced NO_2 gas sensing of a single-layer MoS2 by photogating and piezo-phototronic effects", Science Bulletin, vol. 64, pp. 128C135, 2019
14. Longfei Wang, Shuhai Liu, Guoyun Gao, Yaokun Pang, Xin Yin, Xiaolong Feng, Laipan Zhu, Yu Bai, Libo Chen, Tianxiao Xiao, Xudong Wang, Yong Qin and Zhong Lin Wang, "Ultrathin Piezotronic Transistors with 2 nm Channel Lengths", ACS Nano, vol. 12, pp. 4903-4908, 2018
15. Xingfu Wang, Yejing Dai, Ruiyuan Liu, Xu He, Shuti Li, and Zhong Lin Wang, "Light-Triggered Pyroelectric Nanogenerator Based on a pn-Junction for Self-Powered Near-Infrared Photosensing", ACS Nano, vol. 11(8), pp. 8339-8345, 2017
16. Yan Zhang, Ying Liu, and Zhong Lin Wang, "Fundamental Theory of Piezotronics", Advanced Materials, vol. 23, pp. 3004-3013, 2012
17. Wenzhuo Wu, Zhong Lin Wang, "Piezotronics and piezo-phototronics for adaptive electronics and optoelectronics", Nature Review Materials, vol. 1:16031, 2016
18. Leonard J. Brillson, and Yicheng Lu, "ZnO Schottky barriers and Ohmic contacts", Jounral of Applied Phyiscs, vol. 109: 121301, 2011
19. R. Landauer, "Spatial Variation of Currents and Fields Due to Localized Scatterers in Metallic Conduction", IBM J. Res. Develop. vol. 1, pp. 223-231, 1957
20. Yuji Ando and Tomohiro Itoh, "Calculation of transmission tunneling current across arbitrary potential barriers", Journal of Applied Physics, vol. 61, pp. 1497-1502, 1987
21. Vahid Qaradaghi, A. Ramezany, S. Babu, J. B. Lee, S. Pourkamali, "Nanoelectromechanical Disk Resonators as Highly Sensitive Mass Sensors", IEEE Electron Device Letters, vol. 39 (11), pp. 1744-1747, 2018
22. Guowei Tao, Bhaskar Choubey, "Variability Induced Sensitivity Degradation in Coupled Nano/Micro Resonant Sensors", IEEE Transactions on Nanotechnology, vol. 17(4), pp. 709-713, 2018
23. Soumya Yandrapalli, David Ruffieux, Luis G. Villanueva, "Three-Dimensional Nano-Acoustic Bragg Reflectors for CMOS Embedded NEMS", IEEE Transactions on Nanotechnology, vol. 16(4), pp. 653-658, 2017
24. Leisheng Jin, Jie Mei, Lijie Li, "Chaos control of parametric driven Duffing oscillators", Applied Physics Letters, vol. 104(13), 134101, 2014
25. F. C. Moon and P.J. Holmes, "A magnetoelastic strange attractor", Journal of Sound and Vibration, vol. 65, pp. 275-296, 1979

26. Hu GongWei; Zhang YuJing; Luo Lu; Yang Yang; Zhang Yan; Wang ZhongLin, "Piezotronic transistors in nonlinear circuit: Model and simulation", SCIENCE CHINA-TECHNOLOGICAL SCIENCES, vol. 58(8), pp. 1348-1354, 2015

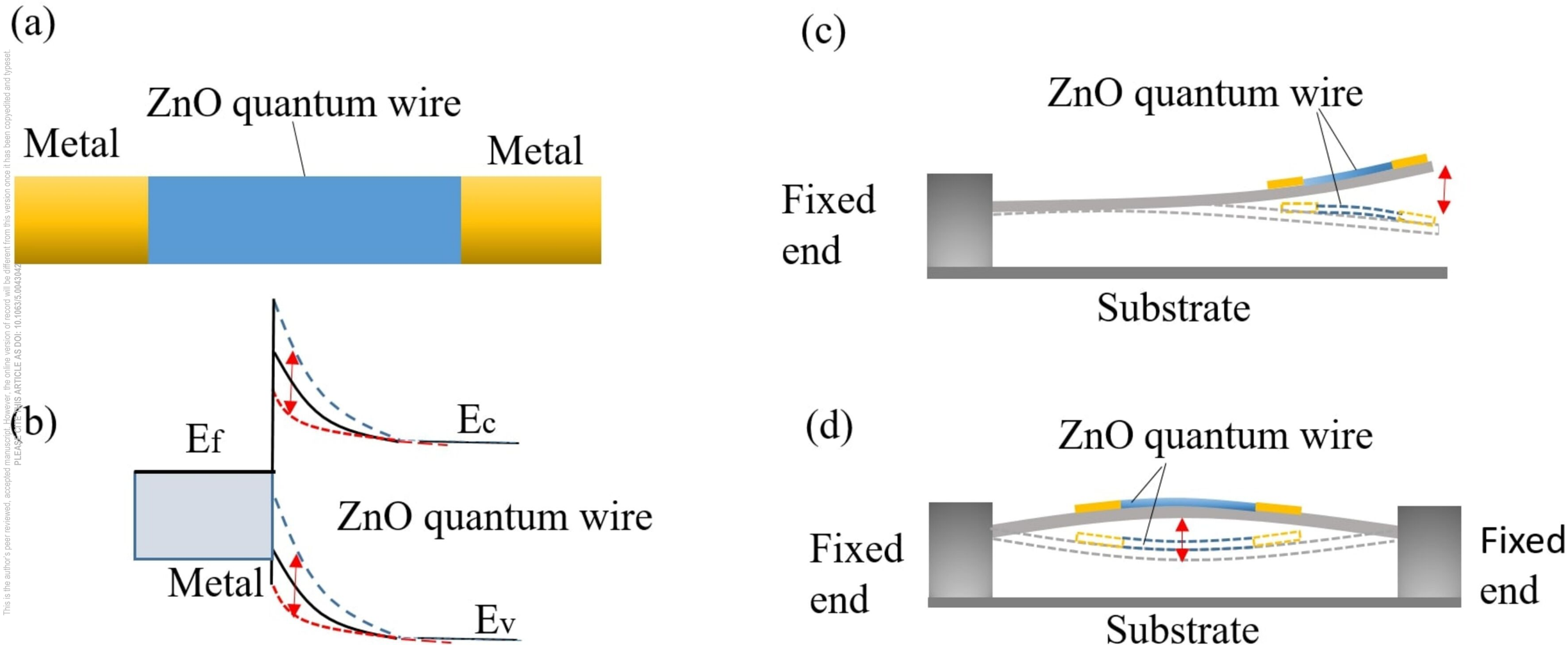

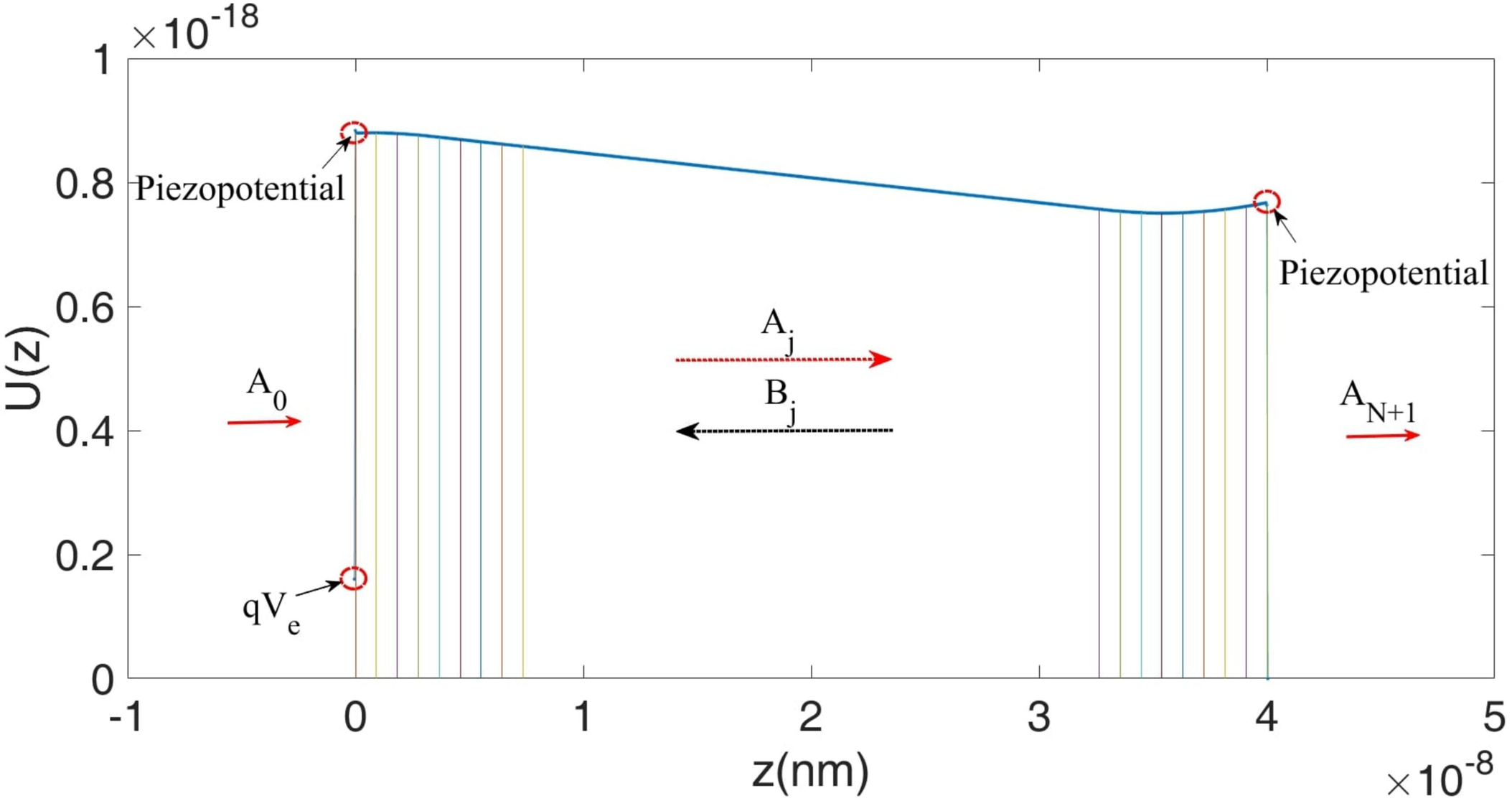

Journal of Applied Physics

ACCEPTED MANUSCRIPT

This is the author's peer reviewed, accepted manuscript. However, the online version of record will be different from this version once it has been copyedited and typeset.
PLEASE CITE THIS ARTICLE AS DOI: 10.1063/5.0043042

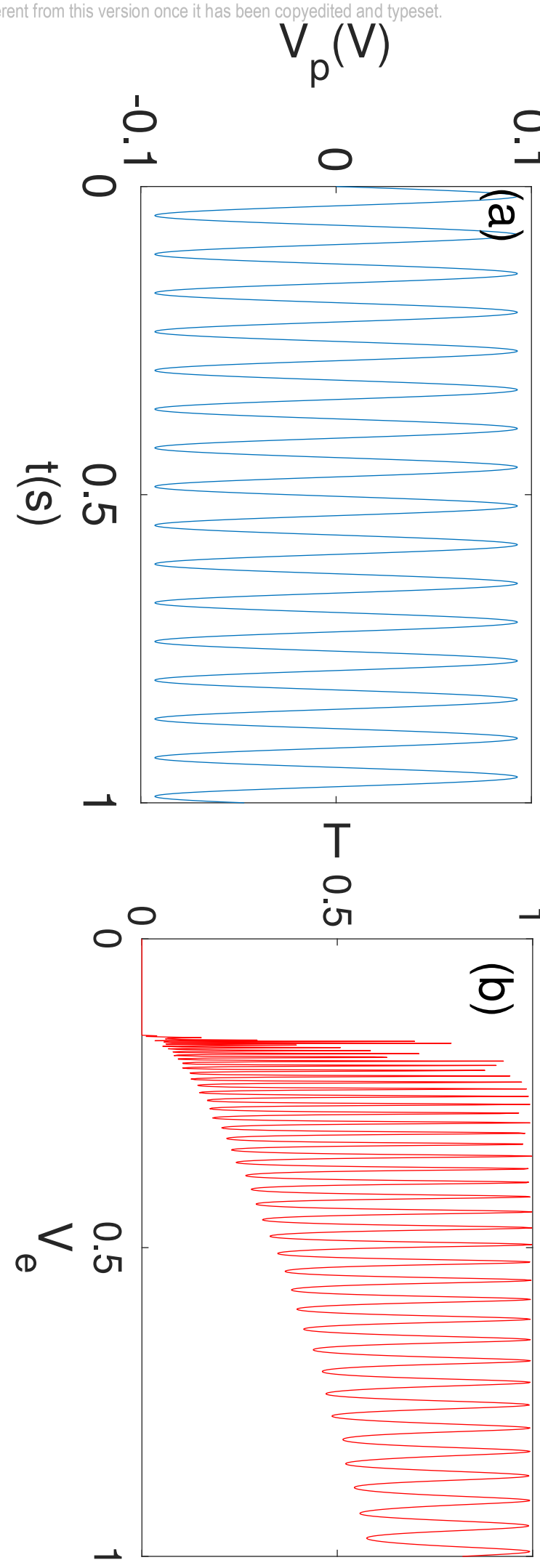

Journal of Applied Physics

Journal of Applied Physics

AIP Publishing
Journal of Applied Physics
ACCEPTED MANUSCRIPT

PLEASE CITE THIS ARTICLE AS DOI: 10.1063/5.0043042

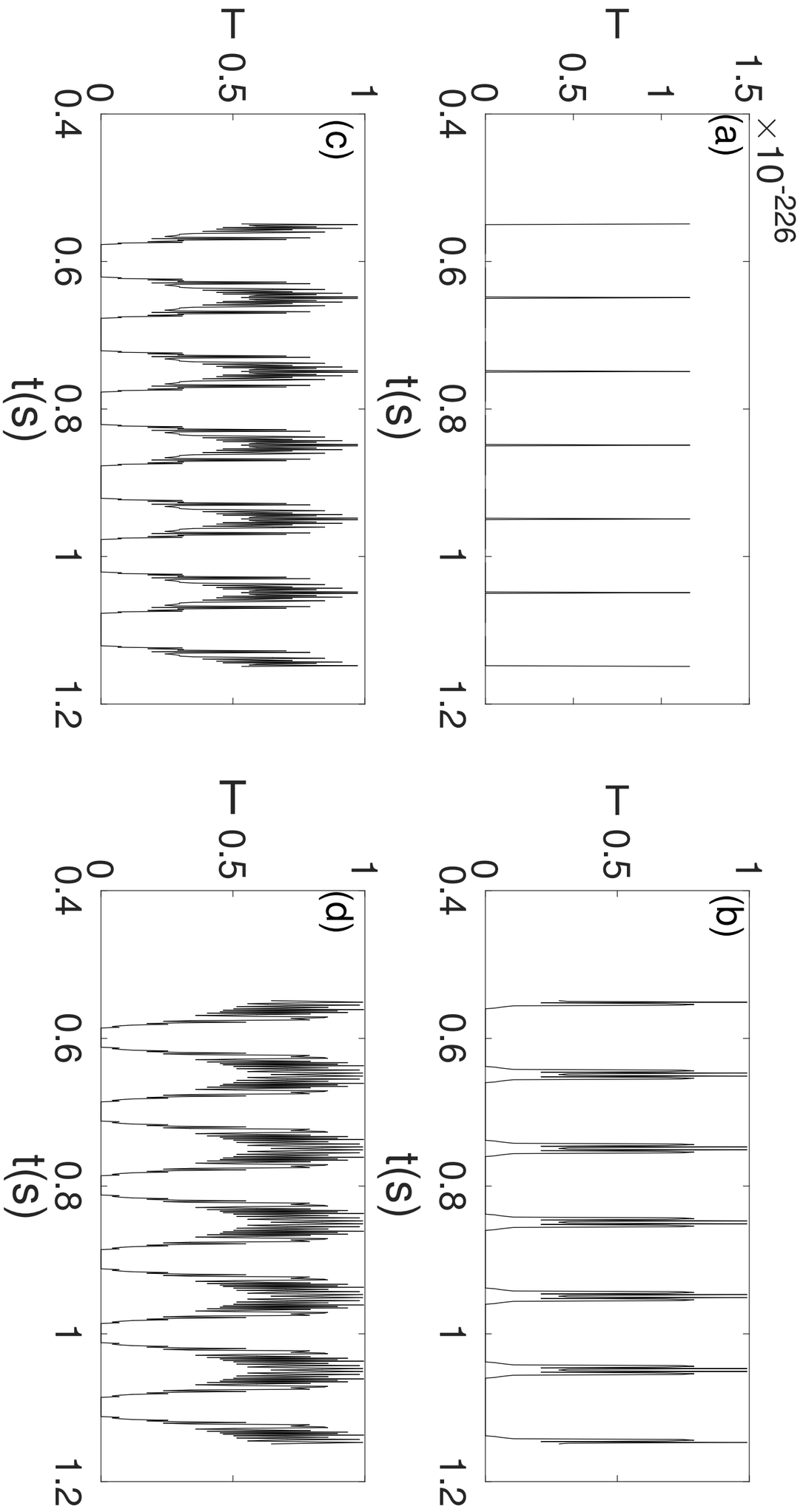

Journal of Applied Physics

AIP Publishing
Journal of Applied Physics
ACCEPTED MANUSCRIPT

PLEASE CITE THIS ARTICLE AS DOI: 10.1063/5.0043042

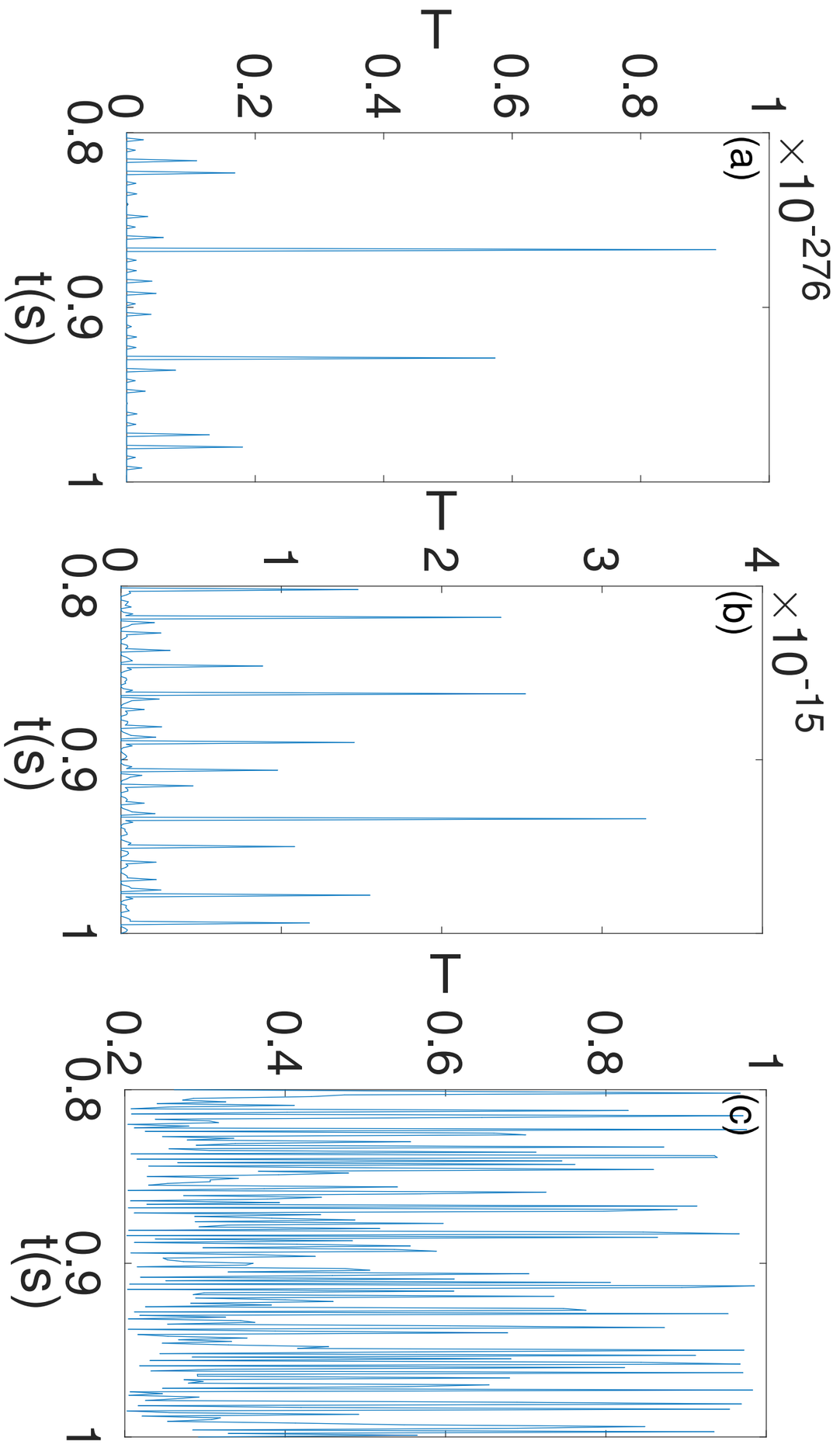

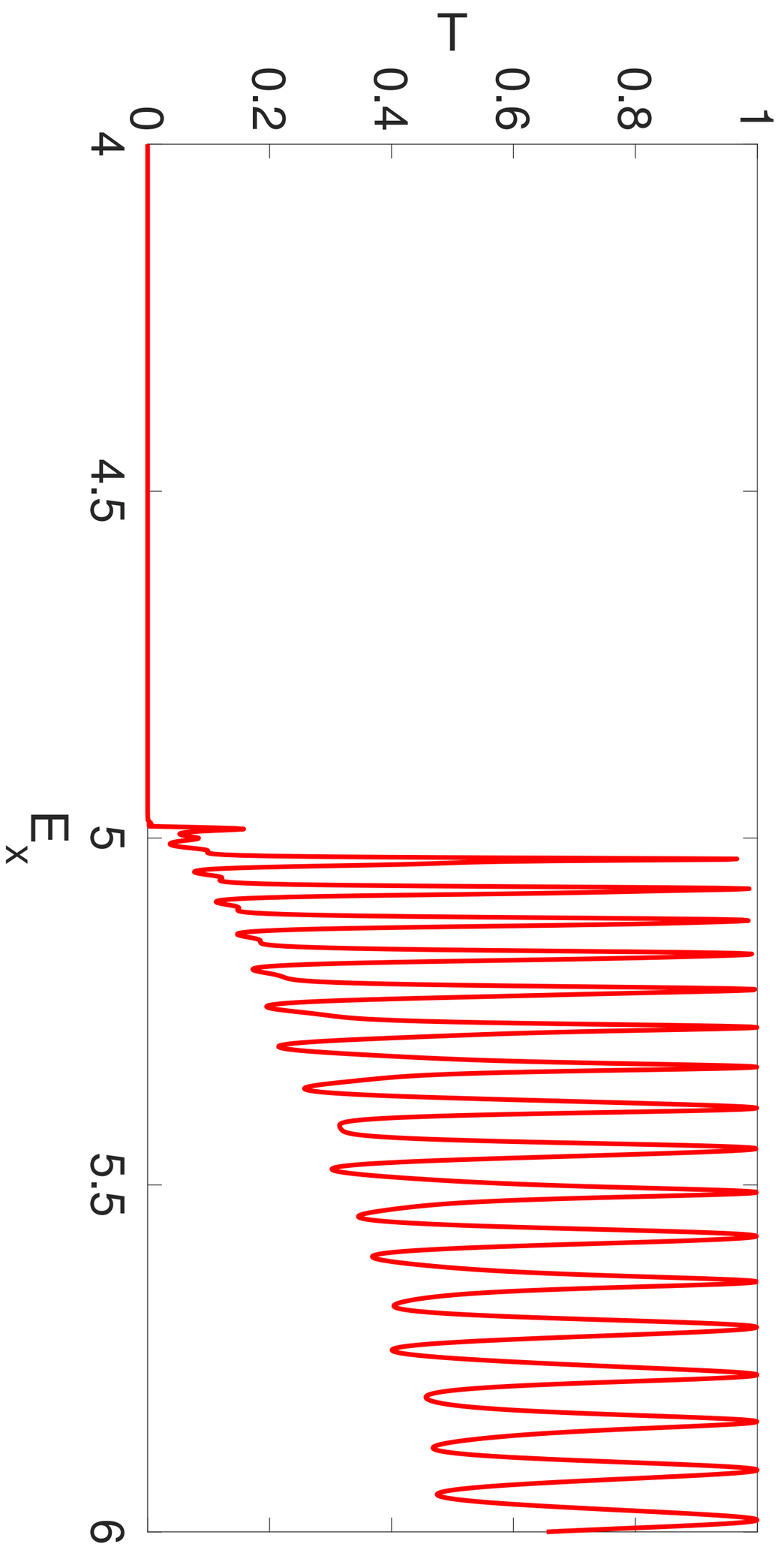

Journal of Applied Physics

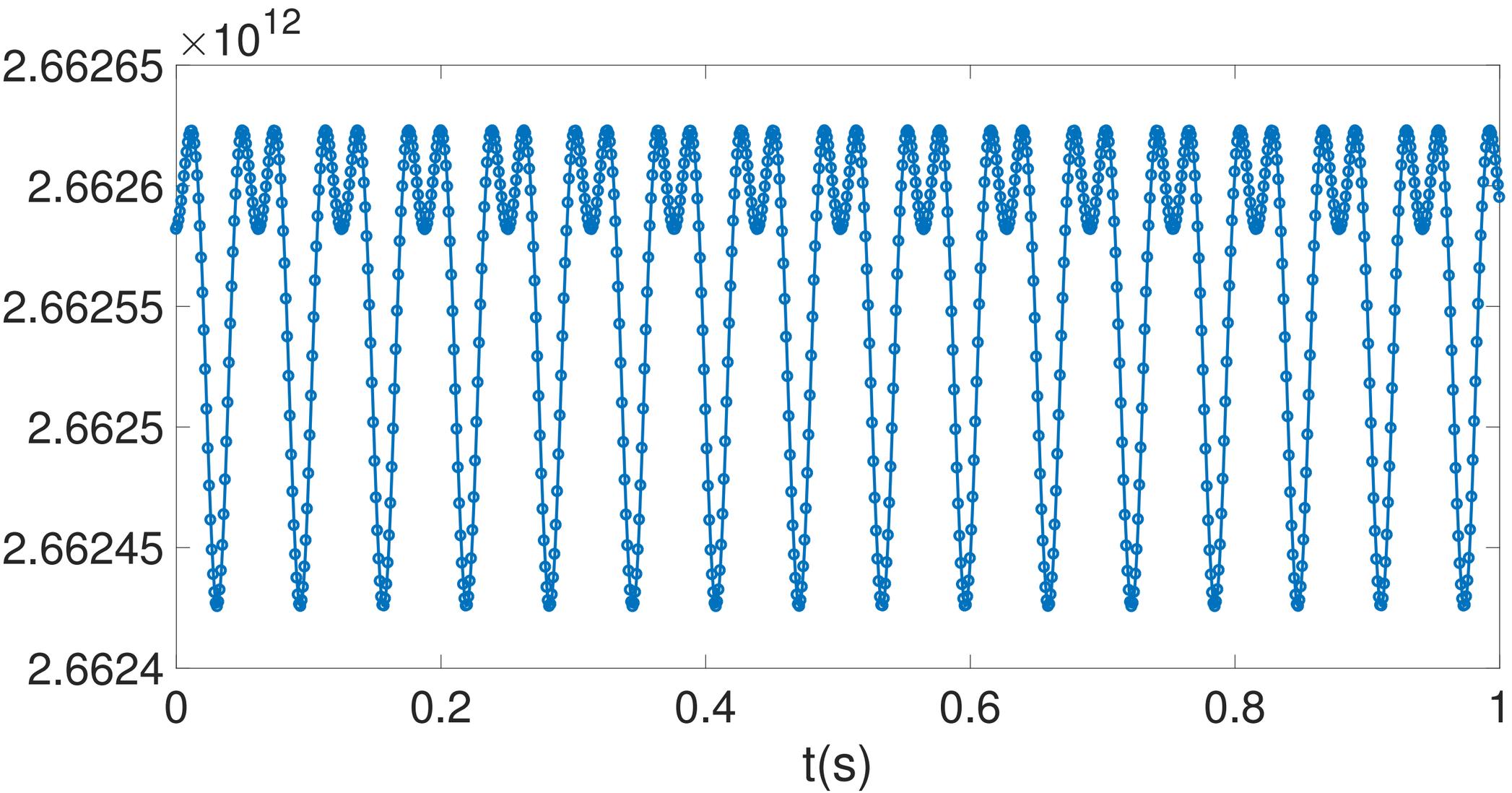

Journal of Applied Physics

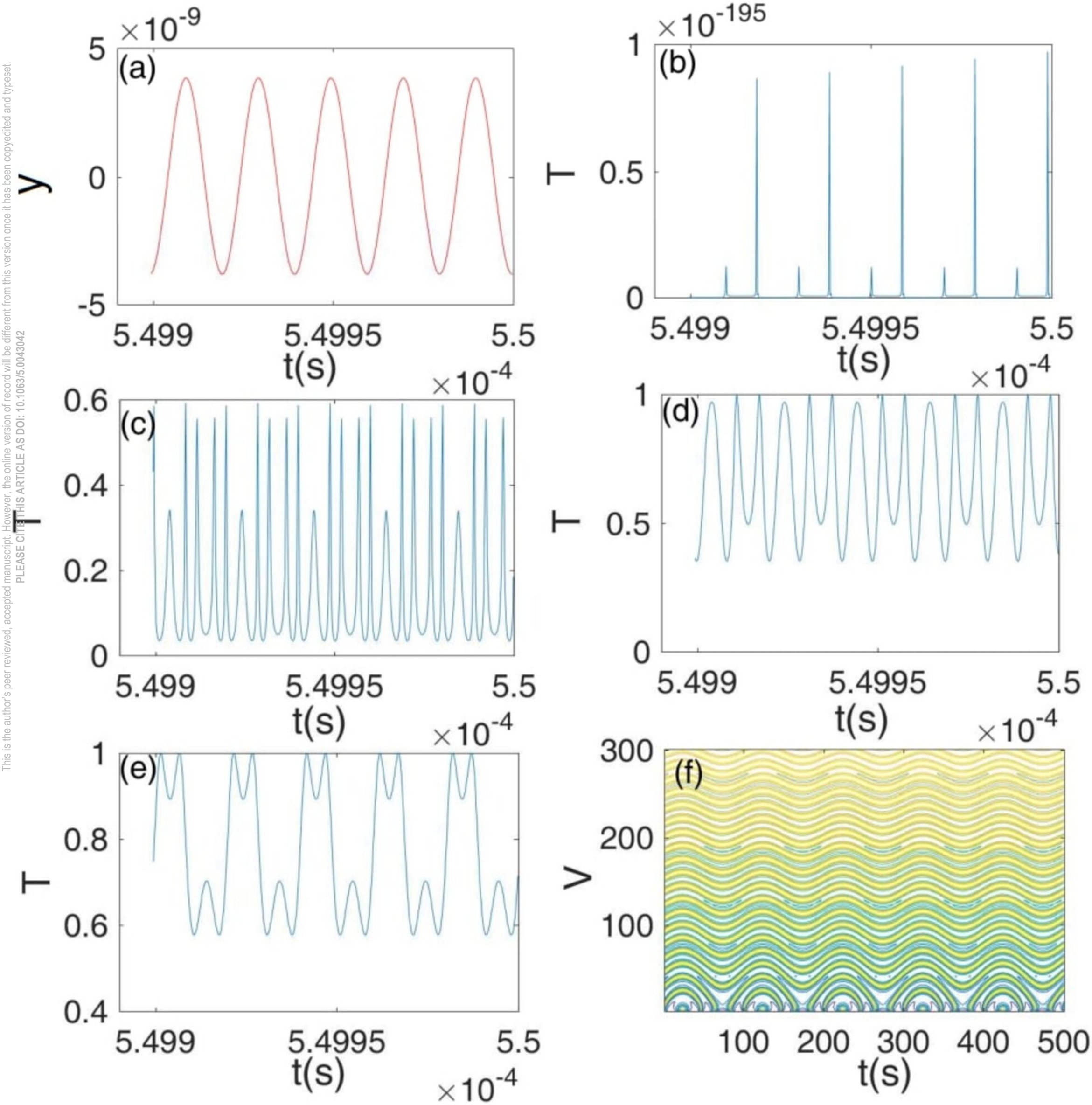

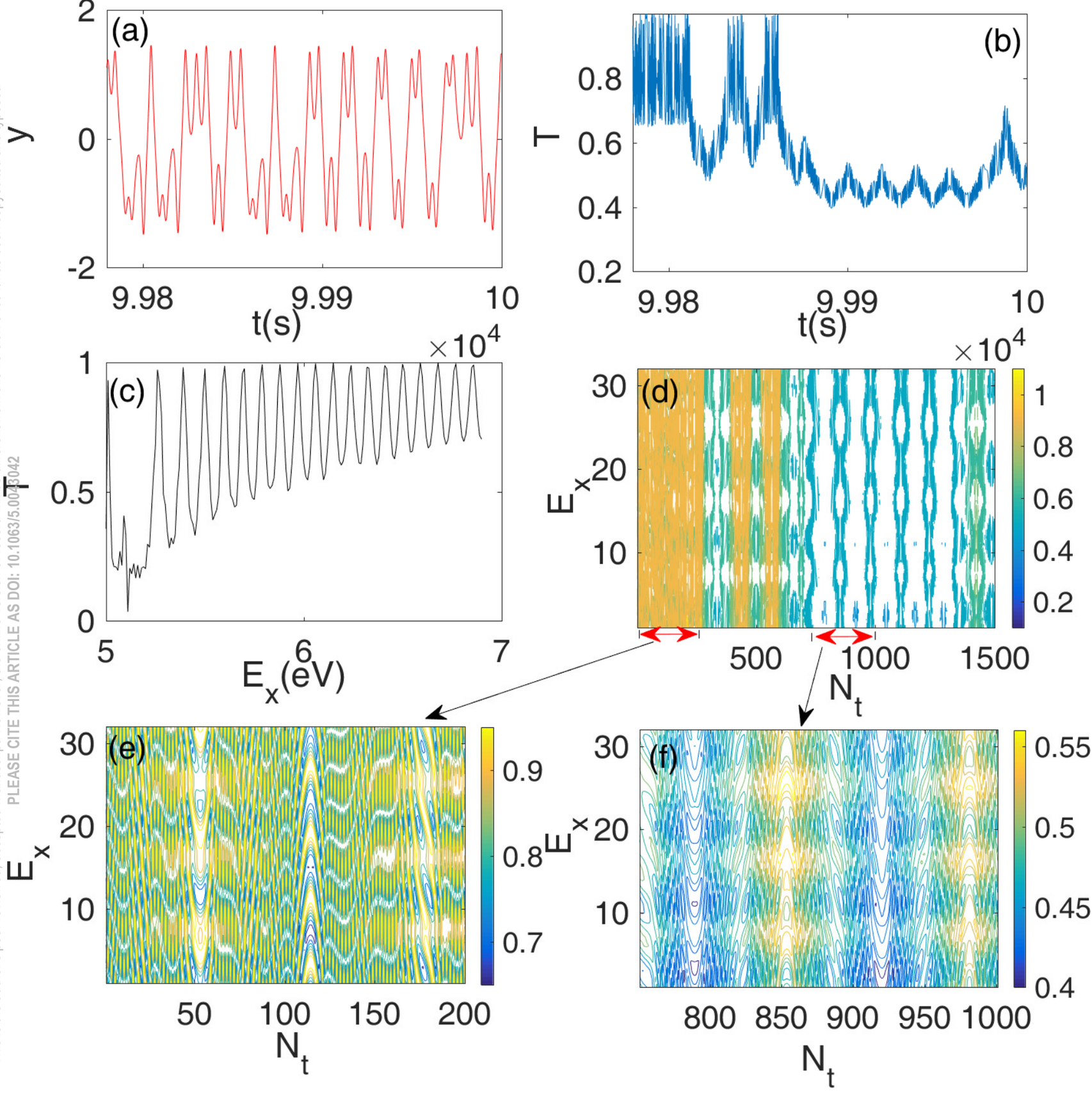

Journal of Applied Physics